Systematic Analysis of Microwave Breast Imaging Detection of Different-Sized Malignant and Benign Tumors

Raquel A. Martins[1], João M. Felicio[1,2], Jorge R. Costa[1,3], Carlos A. Fernandes[1]
[1] Instituto de Telecomunicações, IST, Universidade de Lisboa, Lisboa, Portugal, raquel.martins@lx.it.pt
[2] Centro de Investigação Naval (CINAV), Escola Naval, Almada, Portugal
[3] ISCTE-Instituto Universitário de Lisboa (ISCTE-IUL), Lisboa, Portugal

***Abstract*—Microwave Imaging (MWI) has been explored as an alternative to conventional breast tumor screening methods. It is acknowledged that benign and malignant tumors can be distinguishable by their architectural features: benign tumors are often round with well-defined margin, while malignant tumors have an ill-defined margin and are micro-lobulated or spiculated. We present a MWI-based systematic analysis of malignant and benign breast tumors of different sizes, to evaluate if its characteristics allow differentiating the images. To this end, we performed measurements on a dry MW setup, using a slot-based antenna in the 2-5 GHz frequency range to scan an anthropomorphic breast phantom. We placed inside eight malignant and benign tumors with 3, 4, …10 mm average radius, one at a time. This study shows that both types of tumors can be detected, but not distinguishable only via MWI. Smaller tumors become harder to detect, the 3 mm tumor being unreliably caught.**

***Index Terms*—breast cancer diagnosis, microwave imaging, gaussian random sphere model, slot-based antenna.**

I. Introduction

Microwave Imaging (MWI) is a technique that has been studied as an alternative to conventional imaging systems for monitoring and detection of breast cancer [1]-[5]. This is due to its advantage of being non-invasive, non-ionizing and potentially low-cost. This new technique may be used in a radar-type configuration [4]-[5] and relies on the contrast of dielectric properties between tissues.

In respect to breast lesion properties, it is recognized that malignant and benign tumors may present the same dielectric properties, due to high concentrations of water [6] which may lead to an incorrect identification of the type of tumor.

However, mammography radiologists studied the main differences between these two types of tumors: a benign tumor presents a well-defined margin and is round, oval, or macro-lobulated; a malignant tumor has an ill-defined margin and is micro-lobulated or has spicules [7].

Most literature evaluating MW breast imaging considers only benign tumors i.e., tumor phantoms with uniform shape, such as spheres or ellipsoids [1]-[5]. In addition, imaging studies where both types of tumors are considered, explore only one-sized tumors [8]. To our knowledge, there is no structured study on MWI for malignant and benign tumors currently in the literature.

Therefore, the objective of this paper is to make a systematic analysis of MWI detection of malignant and benign breast tumors with different sizes and analyze if their architectural features can somehow produce differentiated images. Moreover, we show the sensitivity of our dry MW setup to small tumors.

II. Experimental Setup

This section briefly describes the MWI experimental setup, fabrication of breast and tumor phantoms and the algorithm used for image reconstruction.

A. Microwave imaging setup

To acquire the breast backscattered signals, we used the MWI setup developed in [5]. As depicted in Fig. 1, the system comprises a Styrofoam base serving as a support to the breast phantom, and an antenna, in turn connected to a Vector Network Analyzer (VNA). This setup represents a contactless and dry MW system since air is the only medium between the antenna and the breast phantom.

(a) (b)

Fig. 1: MW setup: (a) XETS antenna directed to a breast phantom placed in a styrofoam base; (b) breast phantom with a malignant tumor placed at (20, -10, -45) mm.

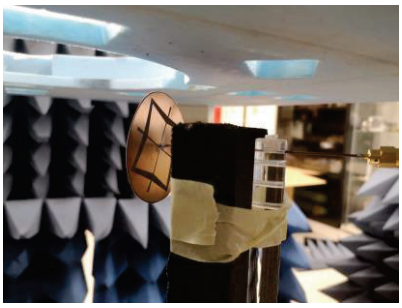

Fig. 2: XETS antenna.

Measurements were performed in the frequency range between 2 GHz and 5 GHz using a crossed exponentially tapered slot-based (XETS) antenna [9], depicted in Fig. 2, scanning around the breast and collecting data at every 9 º. This study adopted a monostatic configuration, meaning that the data for analysis is the complex-valued input reflection $S_{11}(f)$ at the antenna port.

This work was performed using only one breast phantom and sixteen tumors (half benign and half malignant) with different average radius. The tumors were placed in a fixed position (x = 20, y = -10) mm inside the breast, one at a time. Tumors and antenna were kept in the same z-plane of -45 mm.

B. Fabrication of phantoms: breast and tumors

This is a preliminary study, therefore, it considers a simplified type of phantom, with homogeneous filling representing adipose tissue only (no fibroglandular tissue) [10]. Although adding the fibroglandular tissue would improve experiment realism, it would also add unwanted confounding factors at this point. The more complex approach will be addressed in a subsequent study.

For the experimental work we used an MRI-derived breast phantom taken from the University Wisconsin-Madison repository (ID: 062204) [11]. We 3D-printed the breast shell with 1.2 mm wall thickness, depicted in Fig. 3, using polylactic acid (PLA, ε_r = 2.75 [12]) on a Ultimaker 3 Extended [13].

In this experiment, the breast skin is represented by the phantom shell, so by PLA. Although PLA does not present the actual dielectric properties of skin, [5] showed that this approximation does not change the nature of MW scattered signals, only its magnitude response. This difference does not affect the study in a critical manner.

To represent the breast, the breast shell was filled with TX-100 which approximates the dielectric properties of fat (adipose tissue), presenting a complex permittivity of 4 - j0.17 at 4 GHz [14]. A thin layer of a common sealant was applied to the PLA surface, to fill any small fissures present in the wall and thus avoid liquid leakage. This is noticed in Fig. 3, where a thicker amount of sealant (yellow appearance) was applied in the nipple region of the breast.

To generate the tumors, we used the Gaussian Random Sphere model, which is widely used by the breast community [15]. To represent benign tumors, we created

(a) (b)

Fig. 3: Printed breast shell taken from the University Wisconsin-Madison repository: (a) top; (b) side.

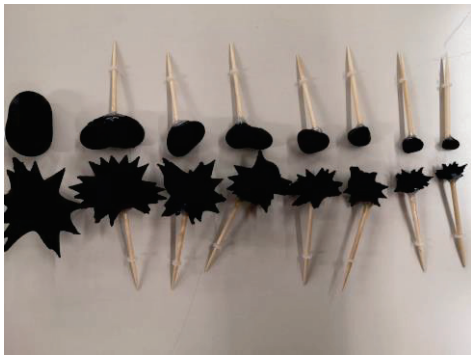

Fig. 4: Printed malignant and benign tumors with average radius of 10, 9, 8, 7, 6, 5, 4 and 3 mm.

eight smooth tumors with different average radius (10, 9, 8, 7, 6, 5, 4 and 3 mm). For malignant tumors, we generated eight spiculated tumors with the same sizes. These tumors, illustrated in Fig. 4, were 3D-printed using conductive PLA filament (commercially known as “protopasta” [16]), which presents a complex permittivity of approximately 20 - j9 at 4 GHz [17]. This material presents lower dielectric properties compared to real tumors, which can lead to a weaker tumor response than the biologic tissue. However, the dielectric contrast is enough to distinguish it from the fat background. Moreover, the use of this material makes it attractive to easily produce complex tumor shapes.

To support the tumors inside the breast container, we used toothpicks to hang them from a star-shaped support placed on top of the breast, as shown in Fig. 1.

C. Microwave image recontruction

Due to its intense response, the skin reflection must be removed from the MW backscattering signals acquired from the experimental setup, prior to image reconstruction of the breast. Hence, we firstly used an adaptive artifact removal algorithm, based on singular value decomposition, and then, reconstructed the image using a wave-migration based algorithm [5].

To assess the quality of the image reconstruction algorithm and tumor detection accuracy we used quantitative figures of merit.

1) Tumor-to-clutter ratio (TCR): compares the maximum intensity corresponding to the tumor response (T)

TABLE I. CALCULATED IMAGING METRICS FOR BENIGN TUMORS

Average Radius Size [mm]	Calculated Imaging Metrics		
	Detected Position (x, y)	*PE [mm]*	*TCR [dB]*
10	(25, 0)	11.2	3.1
9	(25, -5)	7.1	0.3
8	(20, -15)	5.0	4.1
7	(20, -10)	0.0	0.6
6	(20, -10)	0.0	0.7
5	(20, -10)	0.0	1.2
4	(20, -15)	5.0	1.2
3	(20, 10)	20.0	0.8

TABLE II. CALCULATED IMAGING METRICS FOR MALIGNANT TUMORS

Average Radius Size [mm]	Calculated Imaging Metrics		
	Detected Position (x, y)	*PE [mm]*	*TCR [dB]*
10	(25, -10)	5.0	2.3
9	(20, -10)	0.0	2.5
8	(25, -10)	5.0	0.1
7	(15, -15)	7.1	4.2
6	(20, -10)	0.0	1.1
5	(20, -5)	5.0	0.3
4	(20, -10)	0.0	0.3
3	(20, 5)	15.0	1.7

and the larger unwanted artifact intensity (clutter - C) occuring in the 2D image being considered:

$$TCR\ [dB] = 10\log_{10}\left[\frac{\max(T)}{\max(C)}\right] \quad (1)$$

2) Positioning error (PE): quantifies the deviation between the position of the detected tumor, $P_{detected}$, and the correct tumor position, P_{tumor} :

$$PE = \|P_{tumor} - P_{detected}\| \quad (2)$$

III. MICROWAVE IMAGING RESULTS

For representation only, we present in Fig. 5 the image reconstruction for breasts phantoms with malignant and benign tumors with average radius of 10, 8, 5, 4 and 3 mm.

The outer white contour marked in the images, identifies the breast shape in the z-plane in which the antenna and tumors are kept. The white circular marker in these figures identifies the actual tumor position and size. Note that the marker does not represent the actual shape of the used tumors shown in Fig. 4.

Additionally, we present in TABLE I and TABLE II the detected tumor position and the PE and TCR imaging metrics calculated for the different sizes of benign and malignant tumors, respectively.

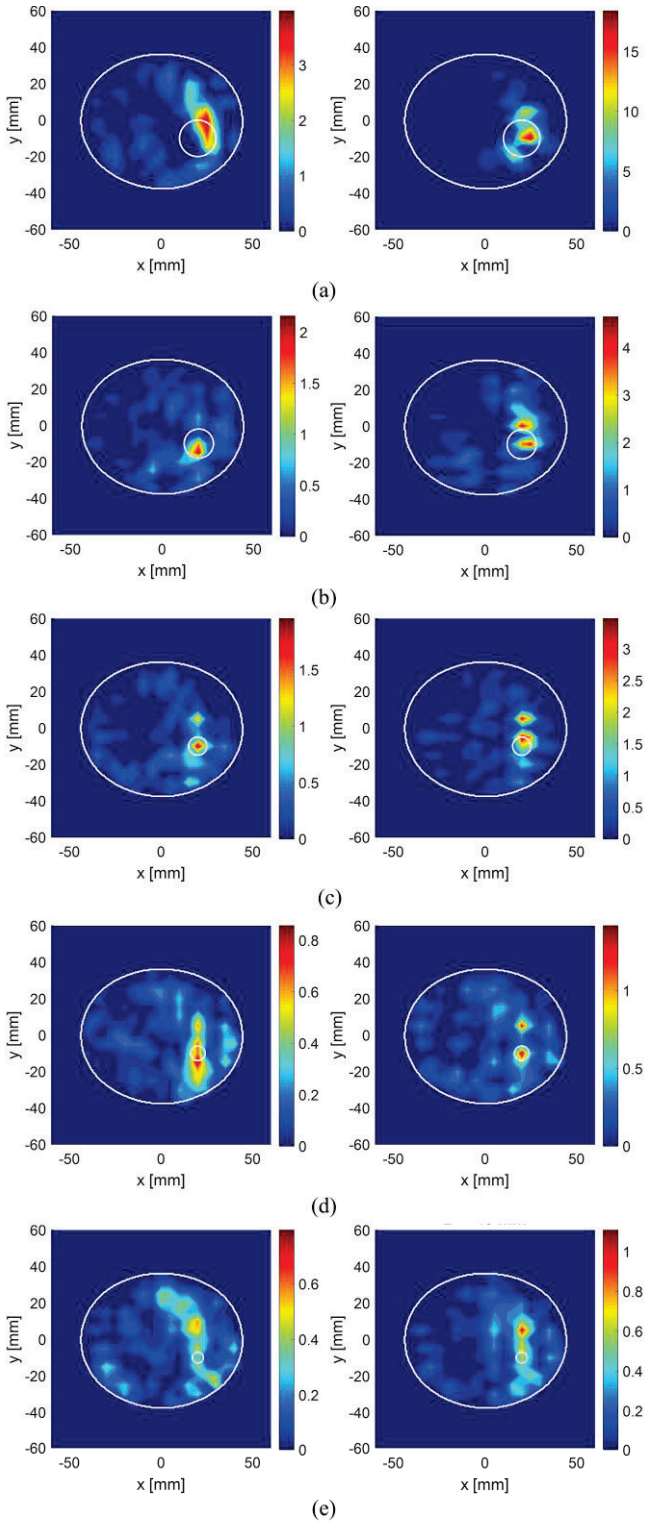

Fig. 5: Two-dimensional images obtained in this study using one breast phantom and benign (left) and malignant (right) tumors of average radius: (a) 10 mm; (b) 8 mm; (c) 5 mm; (d) 4 mm; (e) 3 mm.

With these results we can confirm that both benign and malignant tumors can be detected using our MWI system.

As expected, when the size of tumors decreases, the detection becomes less reliable, however in this test, only the 3-mm case showed a significant shift in the position of the tumor with PE = 20 mm and PE = 15 mm for the benign and malignant tumor, respectively. This gives a measure of our dry setup sensitivity.

It is also clear that in some MW images e.g., in Fig. 5 c), the tumor intensity response is split in smaller clusters. It is this effect that promotes the variability of the calculated TCR for the different tumors.

In respect to discrimination between smooth (benign) and spiculated (malignant) tumors, MWI results do not seem to present a consistent pattern difference. This classification requires other type of complementary signal processing.

IV. Conclusions

The objective of this paper was to present a systematic MWI analysis of malignant and benign breast tumors placed in anthropomorphic phantoms, to evaluate the smallest detectable size for the two kinds of tumors, and to investigate if MWI is sensitive to the different morphological characteristics. We performed the measurements in a dry MW setup, using a XETS antenna to scan the breast phantom. The average radius of the tested tumors was 10, 9, 8, 7, 6, 5, 4 and 3 mm, measured one at a time.

Both types of tumors were detected down to 4-mm radius size. The 3-mm tumor did not produce a reliable detection, this being the detection limit for our MWI setup. Moreover, MWI results showed that malignant and benign tumors cannot be discerned only with this technique.

A future work shall consider new complementary techniques to increase the resolution and to help with the classification of breast tumors. Additionally, the study shall be extended to include the fibroglandular tissue.

Acknowledgment

This work was funded by Fundação para a Ciência e Tecnologia (FCT) under the national project UIDB/50008/2020 and the PhD scholarship number SFRH/BD/144961/2019. In addition, the authors thank the University of University of Wisconsin-Madison for giving access to the MRI-breast model repository.

References

[1] H. Song, et. al, “UWB microwave breast cancer detection with MRI-derived 3-D realistic numerical breast model," *2015 IEEE International Symposium on Antennas and Propagation & USNC/URSI National Radio Science Meeting*, pp. 544-545, July 2015.

[2] E. C: Fear, et al., “Confocal microwave imaging for breast cancer detection: localization of tumors in three dimensions,” *IEEE Trans. Biomed. Eng.*, vol. 49, no. 8, pp. 812-822, Aug. 2002.

[3] E. J. Bond, et al., “Microwave imaging via space-time beamforming for early detection of breast cancer,” *IEEE Trans. Antennas Propag.*, vol. 51, no. 8, pp. 1690-1705, Aug. 2003.

[4] M. Klemm, et al., “Microwave radar-based differential breast cancer imaging: imaging in homogeneous breast phantoms and low contrast scenarios,” *IEEE Trans. Antennas Propag.*, vol. 58, no. 7, July 2010.

[5] J. M. Felício, et al., “Microwave Breast Imaging using a Dry Setup,” *IEEE Trans. Comput. Imaging*, vol. 6, no. 1, pp. 167-180, Jan., 2020.

[6] M. Lazebnik, et al., “A Large-Scale Study of the Ultrawideband Microwave Dielectric Properties of Normal, Benign and Malignant Breast Tissues Obtained from Cancer Surgeries,” *Physics in Medicine and Biology*, vol. 52, pp. 6093–6115, 2007.

[7] A. T. Stravos, et al., “Solid breast nodules: use of sonography to distinguish between benign and malignant lesions,” *Radiology*, vol. 196, no. 1, pp. 123-134, 1995.

[8] H. Zhang, "Microwave Imaging for Breast Cancer Detection: The Discrimination of Breast Lesion Morphology," in *IEEE Access*, vol. 8, pp. 107103-107111, 2020.

[9] J. M. Felício, et al., “Antenna Design and Near-field Characterization for Medical Microwave Imaging Applications,” *IEEE Trans. Antennas Propag.*, vol. 67, no. 7, pp. 4811 - 4824, July, 2019.

[10] "Anatomy of the Breast", *Memorial Sloan Kettering Cancer Center*, 2020. [Online]. Available: https://www.mskcc.org/cancer-care/types/breast/anatomy-breast. [Accessed: 30- Sep- 2021].

[11] M. J. Burfeindt, et al., "MRI-derived 3D-printed breast phantom for microwave breast imaging validation," *IEEE Antennas and Wireless Propagation Letters,* vol. 11, pp. 1610-1613, 2012.

[12] J. M. Felicio, et al., “Complex permittivity and anisotropy measurement of 3D-printed PLA at microwaves and millimeter-waves,” *2016 22nd International Conference on Applied Electromagnetics and Communications* (ICECOM), pp. 1-5, 2016.

[13] "Professional 3D printing made accessible | Ultimaker", ultimaker.com, 2020. [Online]. Available: https://ultimaker.com/. [Accessed: 15- Oct- 2020].

[14] N. Joachimowicz, et al., ‘‘Breast phantoms for microwave imaging,’’ *IEEE Antennas Wireless Propag. Lett.*, vol. 13, pp. 1333–1336, 2014.

[15] K. Muinonen, “Introducing the Gaussian Shape Hypothesis for Asteroids and Comets,” *Astronomy and Astrophysics*, vol. 332, pp. 1087-1098, 1998.

[16] "Proto-pasta Brand 3D Printer Filament - Made in USA by Protoplant Inc", ProtoPlant, makers of Proto-pasta, 2020. [Online]. Available: https://www.proto-pasta.com/. [Accessed: 15- Oct- 2020].

[17] B. Faenger, et al., “Breast phantom with a conductive skin layer and conductive 3D-printed anatomical structures for microwave imaging,” *2017 11th European Conference on Antennas and Propagation* (EUCAP), pp. 1065-1068, 2017.